SEPTEMBER 20, 1968 THROUGH MARCH 20, 1969

COORDINATED SCIENCE LABORATORY

SEMIANNUAL PROGRESS REPORT NO. 1

JPL CONTRACT No. 952383

W. DALE COMPTON

UNIVERSITY OF ILLINOIS – URBANA, ILLINOIS

Investigation of the Luminescent Phenomena of High Resistivity Silicon and Study of Electrical Characteristics of Tunneling into Low Resistivity Silicon

Semi-Annual Progress Report

20 September through 20 March, 1969

JPL 952383

Principal Investigator

W. Dale Compton

15 April 1969

Introduction

This report will summarize activities in four major research areas. Although substantial progress has been made in each of these during the past six months, measurements are still in progress and final conclusions are not possible at this time. The areas of research are:

1) The study of the influence of uniaxial stress and temperature upon the high resolution luminescence spectra of electron irradiated silicon.

2) The study of the effects of lithium dopant upon the spectra of the recombination luminescence of irradiated silicon.

3) The thermal stability of the defects that are responsible for the recombination luminescence in irradiated silicon.

4) The influence of irradiation upon the electron tunneling characteristics of highly doped silicon.

Facilities and Equipment

Two optical systems are being used for the studies of the luminescence. The high resolution system employs an 0.75 meter Engis spectrometer, a high sensitivity PbS detector and both a strip chart and a digital recording system. The digital system is most useful when complete spectra are taken which must be corrected for the variations in system's response as a function of wavelength. The strip chart system is most useful when one is looking at the effects of stress and temperature upon a narrow spectral range of the system.

As will be seen on the data presented below, resolutions of less than 0.001 eV are easily attained with an excellent signal-to-noise.

The second optical system is of lower resolution and employs an 0.5 meter Jarrell-Ash monochromator. This is the system that was used previously by Robert Spry in the initial study of the recombination luminescence of irradiated silicon. Although considerable data have been taken with this system, the signal-to-noise at moderate resolution was never as high as was desired. A new detector system has been developed using optics that provide a smaller image, thus allowing the use of a smaller detector. The signal-to-noise is expected to be about five times better than before. This system is just now being completed.

The tunneling measurements are being made with a conventional system that measures di/dV vs. V and d^2i/dV^2 vs. V and displays these on an x-y recorder. Samples are made by cleavage in air or in high vacuum. Dots of lead or indium are then evaporated on the cleaved surface and current flow measured between the dots and the base material. The samples are immersed in liquid helium. Temperature is measured with a calibrated germanium thermometer.

Measurements of the luminescent spectra are made with the samples mounted onto a cold finger in a liquid helium dewar. The dewar used with the high resolution spectrometer has a variable temperature system and a stress mechanism that was to allow the application of known amounts of uniaxial stress of samples. The stress system did not yield reproducible results. Stress results

presented in this report were obtained by glueing samples to a copper sample holder. Since copper has a thermal contraction that is almost a factor of ten greater than that of silicon, the cooling of this system results in the application of a significant amount of stress.

The low temperature dewar for the lower resolution spectrometer system operates at fixed temperatures as determined by the coolants.

Results

Luminescent Studies

High Resolution Spectra

Figure 1 reproduces data that were taken by Robert Spry of the spectrum of the recombination luminescence of silicon irradiated with 10^8 Roentgen of Co^{60}.[1] As indicated on the figure, a resolution between 0.010 and 0.005 eV was used for this measurement. On the basis of the energy of the peaks from the principal zero phonon lines, A or C, the lines labeled B, D and E were tentatively assigned to transitions that result from phonon assisted transitions with TA and TO phonons involved.

The results of the higher resolution measurements are shown in partial form in Fig. 2. Lines B, D and E are presented with a spectral resolution of between 0.001 and 0.0005 eV, a factor of about ten better than was used in Fig. 1. The importance of this measurement is the observation that these lines have the same half width as the zero phonon lines A and C. Thus, it is likely that these are also zero phonon lines and that they do not arise from phonon assisted transitions.

The earlier data were taken with the sample held to a copper

sample holder with vacuum grease. As will be shown below, this can introduce substantial strain into the crystal thereby tending to broaden and shift the peak position of some of the sharp lines. Lines A and C, when measured without stress, are located at 0.975 and 0.795 eV, respectively. The difference in the position and width of line B between the previous and present measurements may be due to the same effects. Additional data are being taken to aid in the determination of the source of these lines.

Uniaxial Stress

The effects of stress upon the band-to-band luminescence in silicon is shown in Fig. 3. Curve a is the band-to-band luminescence with no applied stress. Curves b to e present the effects of stress and temperature. The stress is essentially compressional in the {100} plane. The light is incident along $\langle 001 \rangle$. Curves b to e are taken at 4.6, 10, 19 and 32^{o}K respectively. Note that the stress results in a splitting of the line and a shifting of the luminescence to lower energy. This result in completely consistent with the splitting and shifting of the silicon conduction band relative to the valence band when a uniaxial stress is applied. A comparison of these results with those of Bulshve[2] indicates that the splitting arises from a stress of approximately 6 x 10^{8} dynes/cm^{2}.

Figure 4 presents some preliminary results on the effects of a compressional stress upon the zero phonon lines A, C, D and E. Curves a, b and c were taken with the compressional stress in the {100} plane, curve d with compressional stress in the {111} plane. Light is incident normal to these planes. Peak A splits into two components. Peak C, D and

E each split into three components. Figure 4b indicates the relative intensity of the three peaks when viewed with polarized light. Note that the poorer resolution is a result of the attenuation by the polaroids.

Although these are preliminary data taken only upon a limited number of samples, these results suggest that this technique will allow the determination of the symmetry of the defect that is responsible for the luminescence. These data will be extended to include other crystallographic orientations for the stress, the degree of polarization of the luminescence and the influence of temperature upon the luminescence, both with and without stress present.

Effect of Lithium Impurity

The material used in these experiments is given in the following table:

	Resistivity Prior to Li Diffusion (Ω-cm)	Lithium Content
N-type Float Zone	70	5.5×10^{17}
N-type Pulled	100	1.5×10^{18}
P-type Float Zone	65	1.2×10^{18}
P-type Pulled	45	1.1×10^{18}

Samples from <u>each</u> of these have been irradiated with 10^{16}, 10^{17} and 10^{18} e/cm^2 having an energy of 3 MeV. Luminescent spectra have been taken after each irradiation with the lower resolution system described above. Note that the representative spectra presented below were taken before

the improvement was made in the detector assembly of this system.

Figure 5 shows the effect of lithium upon the recombination luminescence of N-type float zone material after irradiation with essentially 4 x 10^{18} e/cm^2. Curve A, taken on material without lithium, presents the usual spectrum with a zero phonon line at 0.97 eV and the family of peaks at lower energy and the line at 0.897 eV that we know from the above is also a zero phonon line. The introduction of the lithium results in a tremendous broadening of this spectrum and the introduction of two new luminescent lines into the spectrum at 1.027 and 1.046 eV as shown in Curve B. The zero phonon line at 0.97 eV is still evident on the large background. The structure at 1.027 and 1.046 is always seen in N-type float zone, P-type float zone and N-type pulled material that contains lithium at the high irradiation levels. It has never been seen in P-type pulled and is never seen in any material free of lithium. In P-type float zone and N-type pulled it is seen after irradiation with 10^{17} e/cm^2.

Although these results are preliminary, the lithium appears to introduce a recombination level that is much closer to the band edge than is found in the lithium free material. Thus, a luminescence has been observed that appears to be determined by the lithium. Its properties and the relationship of the defect responsible for it and the defects responsible for the other luminescent emission is yet to be determined.

Absolute measurements of luminescent intensity as a function of irradiation level are very difficult to make, as a result of the

etching techniques that must be used. A threshold appeared to exist for the irradiation needed to produce luminescence. The intensity of the luminescence irradiations below 10^{16} e/cm^2, if present at all, was barely above the noise level. It is hoped that the increased sensitivity of the system will allow a better measure of this threshold effect.

A somewhat different effect of the lithium is seen in Fig. 6 for an N-type pulled sample with lithium after irradiation with 10^{17} e/cm^2 of 2 MeV. Note that the instrumental resolution is substantially poorer in Fig. 6 than in Fig. 5. Of particular interest in this case is the luminescence at low energy that appears to show no structure, at least within this noise level and resolution. Additional measurements are certainly needed to establish the origin of this spectrum.

Although luminescent spectra have been measured on electron irradiated samples of all of the materials prior to lithium doping that are listed in the table above, only curve A of Fig. 5 is presented for the non-lithium doped material. Most of the detailed features of the data as presented by Spry and Compton[1] for neutron and gamma-ray bombardment have been confirmed for electron irradiations. Several observations have been made, however, that will need to be examined more closely with the more sensitive system. For each material type, the intensity of the luminescence appears to be significantly lower after irradiations with 10^{18} e/cm^2 that it was after irradiation with 10^{17} e/cm^2. In N-type pulled, significant luminescence resulting from recombination via the defects was seen after irradiation with 10^{14} e/cm^2, 3 MeV. Thus, the sensitivity of formation

of the defects giving rise to the 0.97 eV and 0.79 eV family of curves is substantially greater than for the same material after lithium diffusion. Finally, a sharp line at about 100 Å higher energy than the 0.79 eV zero phonon line has been seen in some samples. This line has also been seen irregularly in gamma ray and neutron irradiated samples. It is not clear at this time what the relevant parameter is for the observation of this line. Similarly, a luminescence peaking at about 0.5 eV has also been observed in some samples of the irradiated N-type pulled material.

The above data have been presented as examples of the survey data that have been taken. The availability of the more sensitive detection system will require that much of these data be taken again so that more definitive answers can be obtained for many of the questions that were left unanswered in the above discussion.

Effect of Thermal Annealing

A survey of the effect of high temperature anneals upon the recombination spectra of the irradiated material has not been completed. Annealing data has been taken on N-type float zone following irradiation with both 10^{16} and 10^{17} e/cm^2 and N-type pulled following irradiation with 10^{16} e/cm^2. Although no systematics of the effects of high temperature annealing can be presented at this type, an example of the effects of such an anneal will be given for N-type pulled material.

The luminescent intensity of an N-type pulled sample was monitored for about seven weeks after irradiation. Both 0.97 eV and 0.79 eV peaks were visible just after irradiation with the 0.79 eV

peak being about a factor of two lower in intensity than the 0.97 eV peak. It was found that upon standing at room temperature that the ratio of the 0.79 eV to the 0.97 eV peak increased to about unity and then gradually decreased to less than 0.1. The spectrum was measured at this time and is shown in Fig. 7. The sample was then annealed at 300°C for 14 hours and the spectrum of Fig. 8 obtained. A tremendous increase in the 0.79 eV peak is seen. The insert, taken at higher resolution shows the line at 100Å to higher energy than the 0.79 eV line. Notice also that the 0.97 eV zero phonon line is no longer seen and that a new family of lines has appeared at slightly lower energy. It is not clear whether this new luminescence results from a new defect created by the anneal or whether this series has simply become evident because of the absence of the stronger 0.97 eV family.

One N-type float zone crystal also has been annealed. The only luminescence seen before anneal, the 0.97 eV zero phonon family, is destroyed and a weak structureless band was seen, stretching from the monochromators low energy limit of 0.70 eV to about 0.97 eV. It is expected that the systematic investigation of the affects of annealing will yield additional information on the relationship of the defects that give rise to the two luminescent patterns at 0.79 and 0.97 eV.

Tunneling in P-Type Silicon

Tunneling measurements have been completed on MOS devices made from degenerate silicon. The data shown in Fig. 9 through 12 were obtained from samples cut from 4 boron doped crystals with impurity concentrations

ranging from 1.8×10^{19} cm^{-3} to 2×10^{20} cm^{-3}. The interaction of tunneling electrons with optical and local-mode phonons is clearly evident in the data. Samples with the highest boron concentration, Fig. 9, exhibit phonon lineshapes that are qualitatively explained in terms of a many body self-energy effect in the semiconductor electrode[3]. Variations in the lineshape with boron concentration (Fig. 10, 11 and 12) leads us to the conclusion that both the electronic self-energy effect and inelastic phonon emission in the barrier must be taken into account in order to adequately describe the observed data.

Figure 9 shows $\frac{di}{dV}$ and $\frac{d^2i}{dV^2}$ data from a sample with a boron concentration of 2×10^{20} cm^{-3}. Positive bias corresponds to raising the Fermi level in the metal with respect to that in the semiconductor. The large positive $\frac{d^2i}{dV^2}$ peaks at positive and negative bias results from the interactions of tunneling electrons with silicon optical phonons of small wave vector. The positive bias peak occurs at 64.2 ± 0.4 mV which is 0.6 mV below the value obtained from Raman scattering for the optical phonon. This discrepancy is believed to be due to phonon dispersion effects. Since the peak gradually shifts with decreasing boron concentration to 64.5 ± 0.4 mV in the lowest doped sample, this explanation would seem to be valid.

At positive bias the interaction with silicon optical phonons results in an <u>increase</u> in the conductance while at negative bias a conductance <u>decrease</u> is observed. The corresponding second derivative structure is approximately symmetrical about zero bias. Inelastic phonon emission in the barrier would have resulted in an <u>increase</u> in conductance in both bias directions and hence antisymmetric peaks in second derivative. This inelastic tunneling

process can therefore be ruled out as the predominant mechanism in this case.

Duke and Davis[4] have calculated the electronic self-energies in degenerate semiconductors due to electron interactions with optical phonons; and the effects of such many-body interactions on the tunneling conductance have been evaluated numerically and compared with these experimental data. The theoretical lineshapes are in qualitative agreement with experiment. The symmetrical $\frac{d^2i}{dV^2}$ structure is thus interpreted as being the result of an electronic self-energy effect due to optical phonon interactions in the semiconductor electrode.

Separated from the optical phonon peaks by about 15 mV is another pair of positive peaks. This structure has been attributed to interactions with boron local mode vibrations. The origin of this structure is clearly established, not only by the energy of the peaks but by their strong dependence upon boron impurity concentration and the details of the splitting of the structure at positive bias. Infrared absorption measurements on boron doped silicon attribute peaks at 76.9 and 79.9 meV to local mode absorption due to isolated B^{11} and B^{10} isotopes.[5] The natural isotopic abundances are 80% B^{11} and 20% B^{10}. The relative heights of the two resolved peaks in forward bias, the separation of the two peaks and the absolute energy of the peaks are all in agreement with the infrared absorption data. The symmetric nature of this structure would again lead us to believe that we are observing the result of a many-body effect in the silicon electrode.

Figures 10, 11, and 12 show tunneling data from samples with progressively decreasing boron content. The boron local mode structure

grows weaker as the boron concentration is decreased and fades entirely at the lowest doping. While the positive bias optical phonon lineshape does not change significantly in these figures, the reverse bias $\frac{d^2i}{dV^2}$ structure undergoes a continuous change from a positive peak at the highest doping level to a step-like structure as the lowest doping level. In contrast to the first three samples, the Fermi degeneracy of the silicon for $N_a = 1.8 \times 10^{19}$ cm^{-3}, (approximately 45 meV), is less than the optical phonon energy; hence, at a positive bias equal to the phonon energy, electrons tunneling from states near the Fermi level of the metal electrode can do so only if they emit a phonon, since these electrons are tunneling into the forbidden gap of the semiconductor. We now have a situation in which inelastic phonon emission must be the dominant mechanism. That the many-body effect must still be considered, however, is implied by the reverse bias lineshape. Similar lineshapes have been observed in heavily doped p-type Ge MOS junctions. Neither mechanism alone predicts such a lineshape, and we feel that more precise calculations, including both the electronic self-energy effect of the optical phonon coupling and inelastic phonon emission in the barrier, would be required to explain this latter lineshape and the variations in lineshape with boron concentration that we have observed in our data.

Preliminary measurements have been made on silicon samples of lower doping than presented in Figs. 9 through 12 with $N_a = 6.5 \times 10^{18}$ cm^{-3}. On these units, the vacuum cleavage was made in a way that

allowed some contamination of the cleavage plane; not enough for an insulating barrier to form but enough to alter the surface state density, producing a higher tunneling barrier and hence measurable resistances. While the superconducting structure of the metal electrode was not seen, a magnetic field dependent conductance minimum was observed at zero bias, as seen in Fig. 13. Also the zero bias conductance minimum was found to be strongly temperature dependent, Fig. 14, and is thought to be the result of a two-step tunneling process. At positive bias, for instance, an electron tunnels into a localized state in the depletion region of the semiconductor and then tunnels into the valence band. Measurements of the temperature dependence over a wider temperature range together with a check of the variation with doping are planned. These experiments should make it possible to clearly establish the origin of the structure. If it is shown to result from localized states, this technique will be used to examine localized defects introduced by radiation.

References

1. R. J. Spry & W. D. Compton, Phys. Rev. 175, 1010 (1968).

2. I. Balslev, Phys. Rev. 143, 636 (1966).

3. E. L. Wolf, Phys. Rev. Letters 20, 204 (1968).

4. L. C. Davis & C. B. Duke, "Tunneling Measurement of Electronic Self Energies Due to Electron (Hole) Interactions with Optical Phonons in Semiconductors," to be published.

5. M. Balkanski and W. Nazarewicz, J. Phys. Chem. Solids 27, 671 (1965).

Figure Captions

Fig. 1. Recombination luminescence in Co^{60} irradiated 100 ohm-cm N-type silicon.

Fig. 2. High resolution spectra of lines labeled B, D and E of Fig. 1.

Fig. 3. Effect of compressional stress in the {100} plane upon the band-to-band luminescence in silicon. 90 ohm-cm P-type pulled.

a) No stress

b)-e) Effect of compressional stress in {100} plane.

b) $4.6^{o}K$

c) $10^{o}K$

d) $19^{o}K$

e) $32^{o}K$

Fig. 4. Effect of compressional stress upon lines A, C, D, and E of the luminescent spectrum in irradiated silicon. 90 ohm-cm P-type pulled irradiated with 4×10^{18} e/cm^2. Curves a, b and c.

a) Line A - $8^{o}K$ - {100} plane

b) Line C - $8^{o}K$ - {100} plane

c) Line D and E - $8^{o}K$ - {100} plane

d) Line C - $8^{o}K$ - {110} plane

Fig. 5. Recombination luminescence of irradiated silicon.

A) N-type float zone 70 ohm-cm

Irradiated with 4.2×10^{18} e/cm^2

B) N-type float zone 70 ohm-cm with $5 \times 10^{17}/cm^3$ of lithium.

Irradiated with 3.5×10^{18} e/cm^2.

Fig. 6. Recombination luminescence on irradiated N-type pulled silicon containing $1.5 \times 10^{18}/cm^3$ of lithium. Irradiated with 10^{17} e/cm^2.

Fig. 7. Recombination luminescence of 100 ohm cm N-type pulled silicon after irradiation with 10^{16} e/cm^2 and room temperature anneal for seven weeks.

Fig. 8. Recombination luminescent spectrum of sample used in Fig. 7 after an anneal at $300^{\circ}C$ for 14 hours.

Fig. 9. $\frac{di}{dV}$ and $\frac{d^2i}{dV^2}$ for indium-silicon junction with silicon doped to $N_A = 2.1 \times 10^{20}$ B/cm^3.

Fig. 10. $\frac{di}{dV}$ and $\frac{d^2i}{dV^2}$ for indium-silicon junction with silicon doped to $N_A = 1.17 \times 10^{20}$ B/cm^3.

Fig. 11. $\frac{di}{dV}$ and $\frac{d^2i}{dV^2}$ for indium-silicon junction with silicon doped to $N_A = 4.2 \times 10^{19}$ B/cm^3.

Fig. 12. $\frac{di}{dV}$ and $\frac{d^2i}{dV^2}$ for indium-silicon junction with silicon doped to $N_A = 1.75 \times 10^{19}$ B/cm^3.

Fig. 13. Temperature dependence of the conductance <u>vs</u>. applied bias for a lower doped sample containing $N_A = 6.5 \times 10^{18}$ B/cm^3.

Fig. 14. Magnetic field dependence of the conductance vs. applied bias for sample shown in Fig. 13.

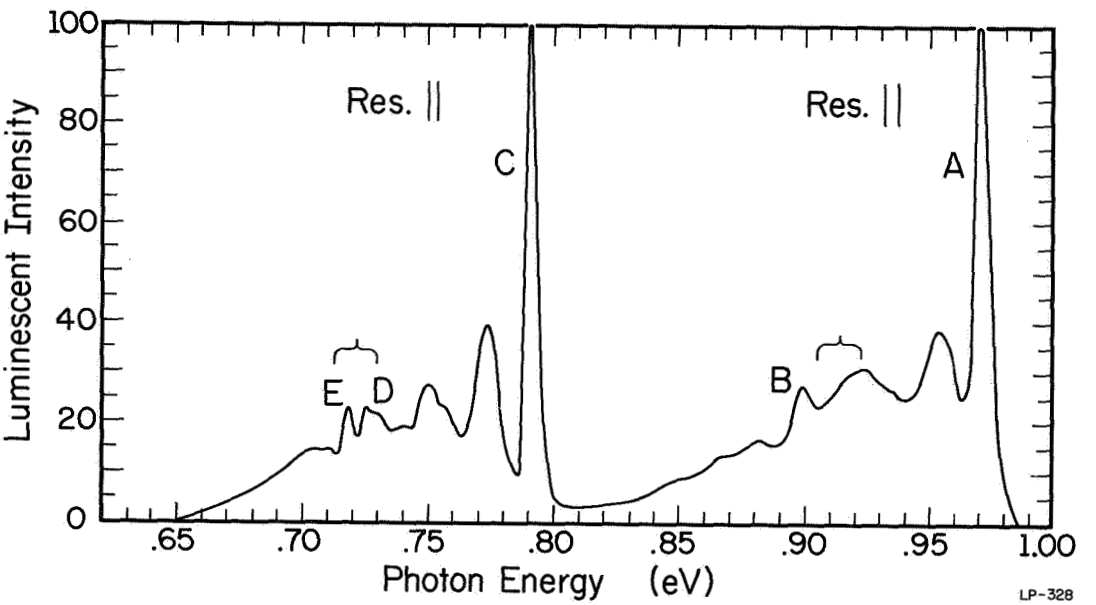
100
80
60
40
20
0
Luminescent Intensity
Res. ||
Res. ||
C
A
E
D
B
.65
.70
.75
.80
.85
.90
.95
1.00
Photon Energy (eV)
LP-328

Figure 1

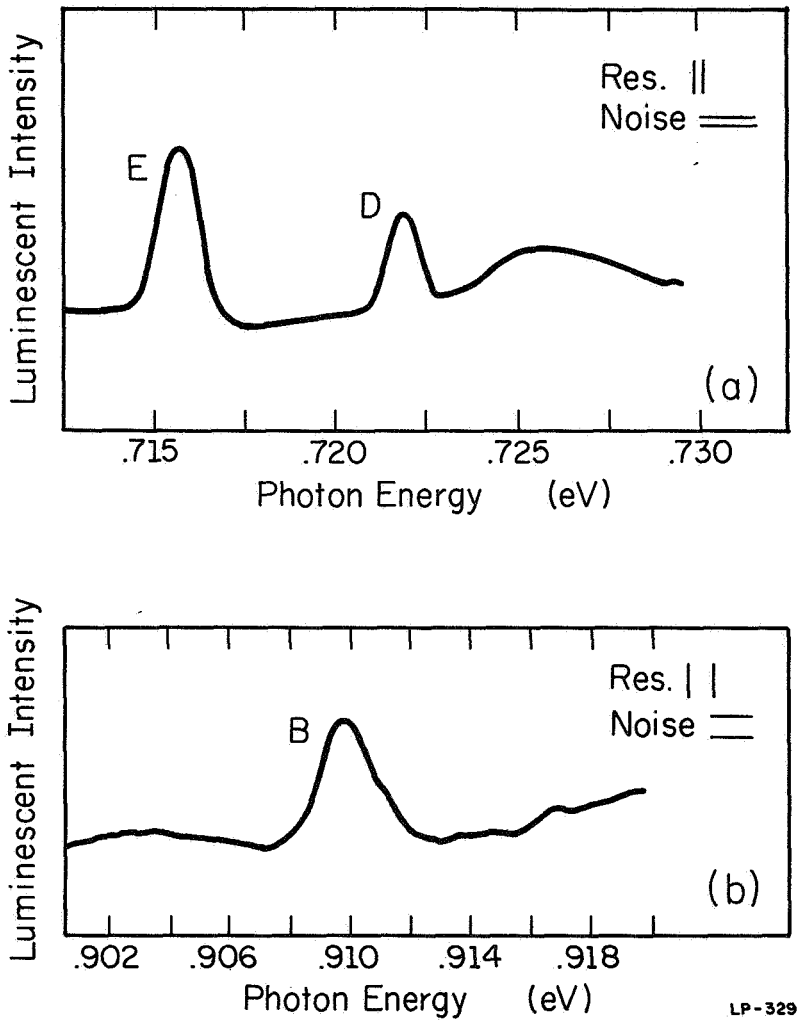
Luminescent Intensity
Res. ||
Noise ==
E
D
(a)
.715
.720
.725
.730
Photon Energy (eV)
Luminescent Intensity
Res. | |
Noise =
B
(b)
.902
.906
.910
.914
.918
Photon Energy (eV)
LP-329

Figure 2

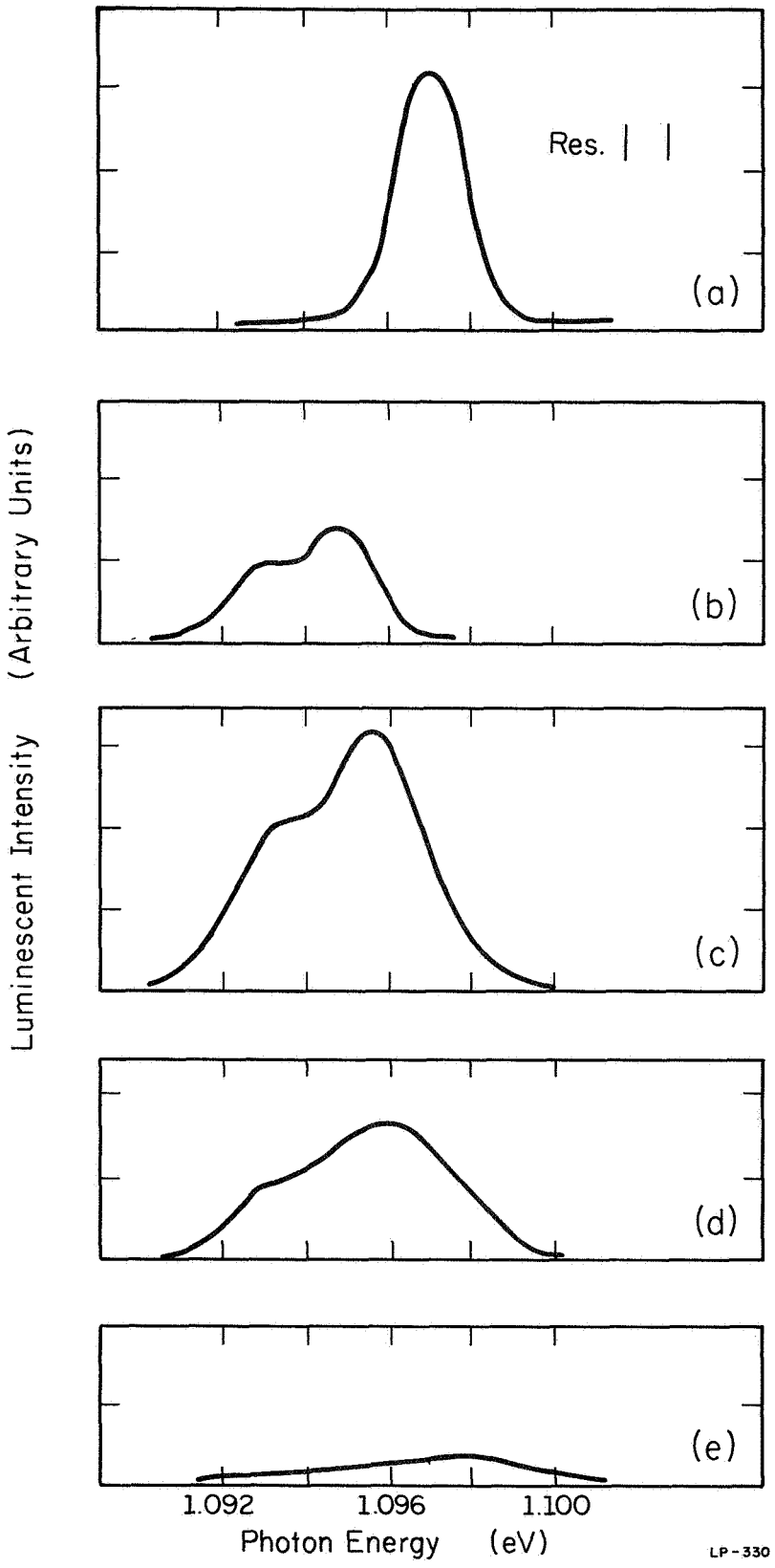
Res.
(a)
(b)
(c)
(d)
(e)
Luminescent Intensity (Arbitrary Units)
1.092
1.096
1.100
Photon Energy (eV)
LP-330

Figure 3

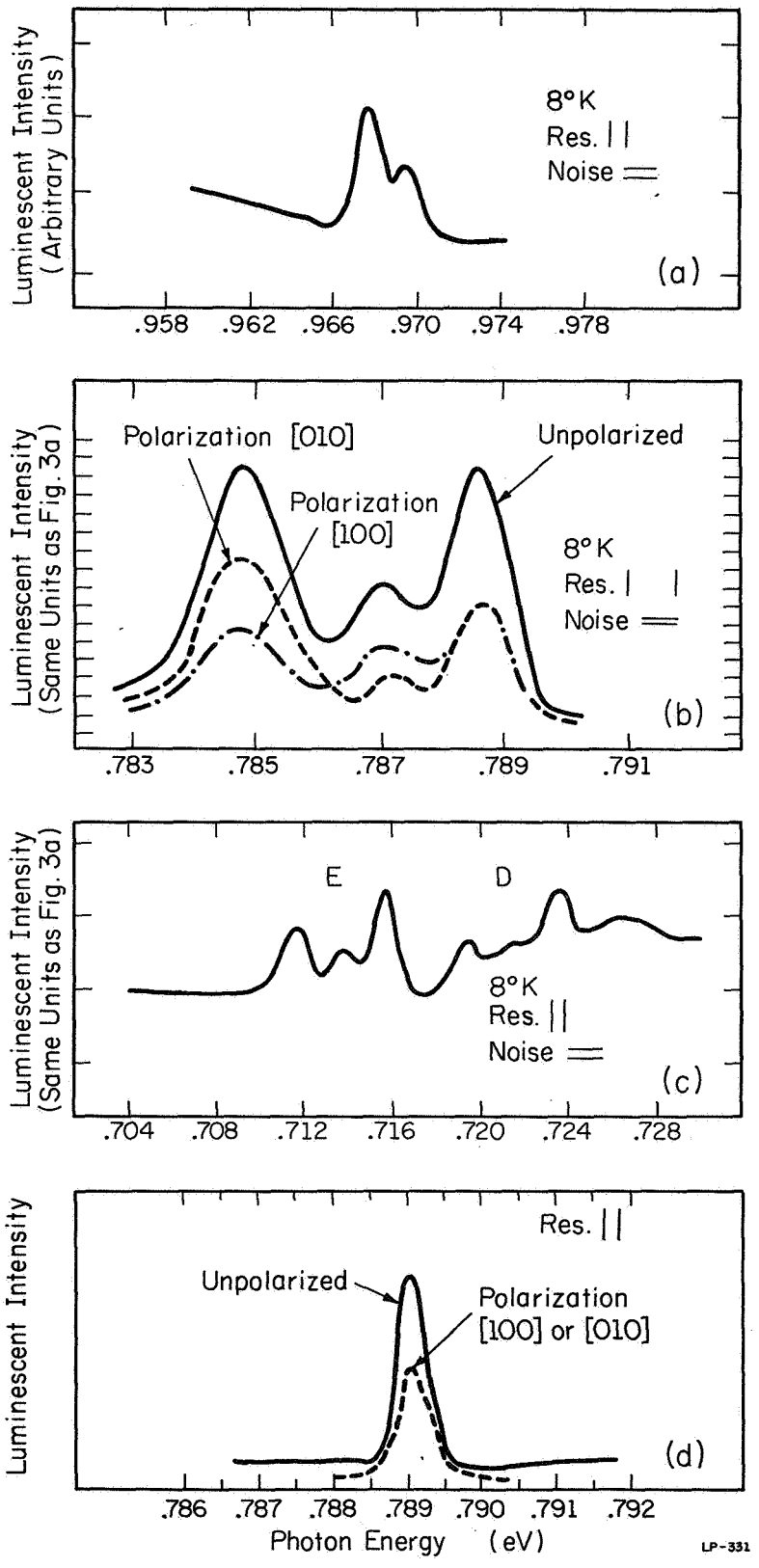
Luminescent Intensity
(Arbitrary Units)
8°K
Res. | |
Noise ═
(a)
.958 .962 .966 .970 .974 .978
Luminescent Intensity
(Same Units as Fig. 3a)
Polarization [010]
Unpolarized
Polarization
[100]
8°K
Res. | |
Noise ═
(b)
.783 .785 .787 .789 .791
Luminescent Intensity
(Same Units as Fig. 3a)
E
D
8°K
Res. | |
Noise ═
(c)
.704 .708 .712 .716 .720 .724 .728
Luminescent Intensity
Res. | |
Unpolarized
Polarization
[100] or [010]
(d)
.786 .787 .788 .789 .790 .791 .792
Photon Energy (eV)
LP-331

Figure 4

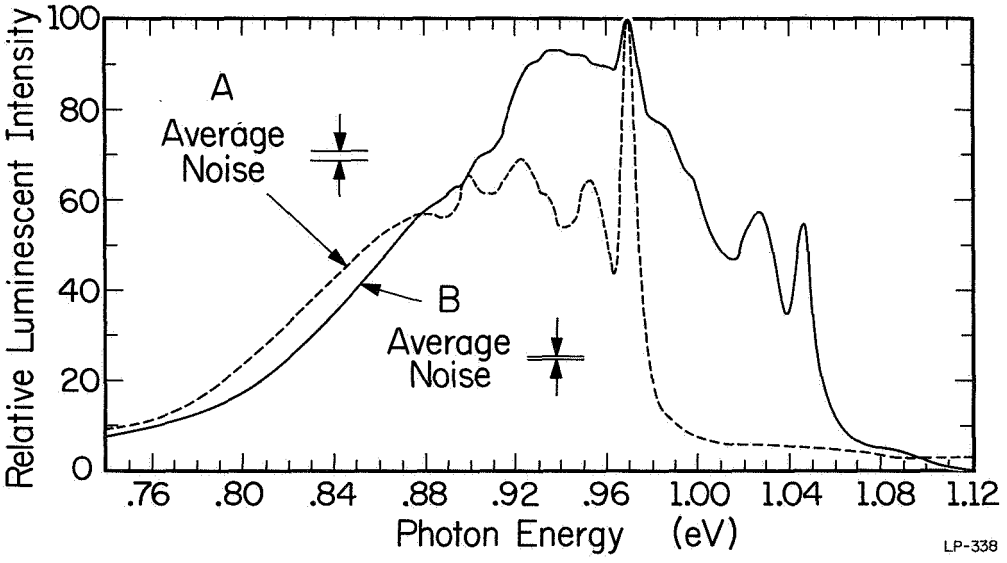
Relative Luminescent Intensity
100
80
60
40
20
0
A
Average
Noise
B
Average
Noise
.76
.80
.84
.88
.92
.96
1.00
1.04
1.08
1.12
Photon Energy (eV)
LP-338

Figure 5

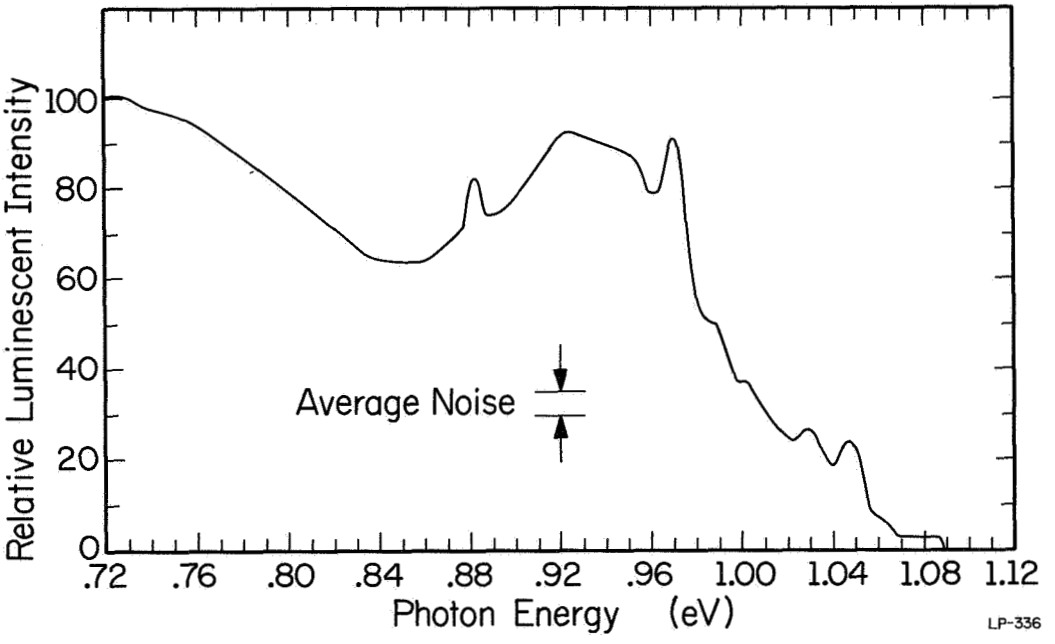
Relative Luminescent Intensity
100
80
60
40
20
0
Average Noise
.72
.76
.80
.84
.88
.92
.96
1.00
1.04
1.08
1.12
Photon Energy (eV)
LP-336

Figure 6

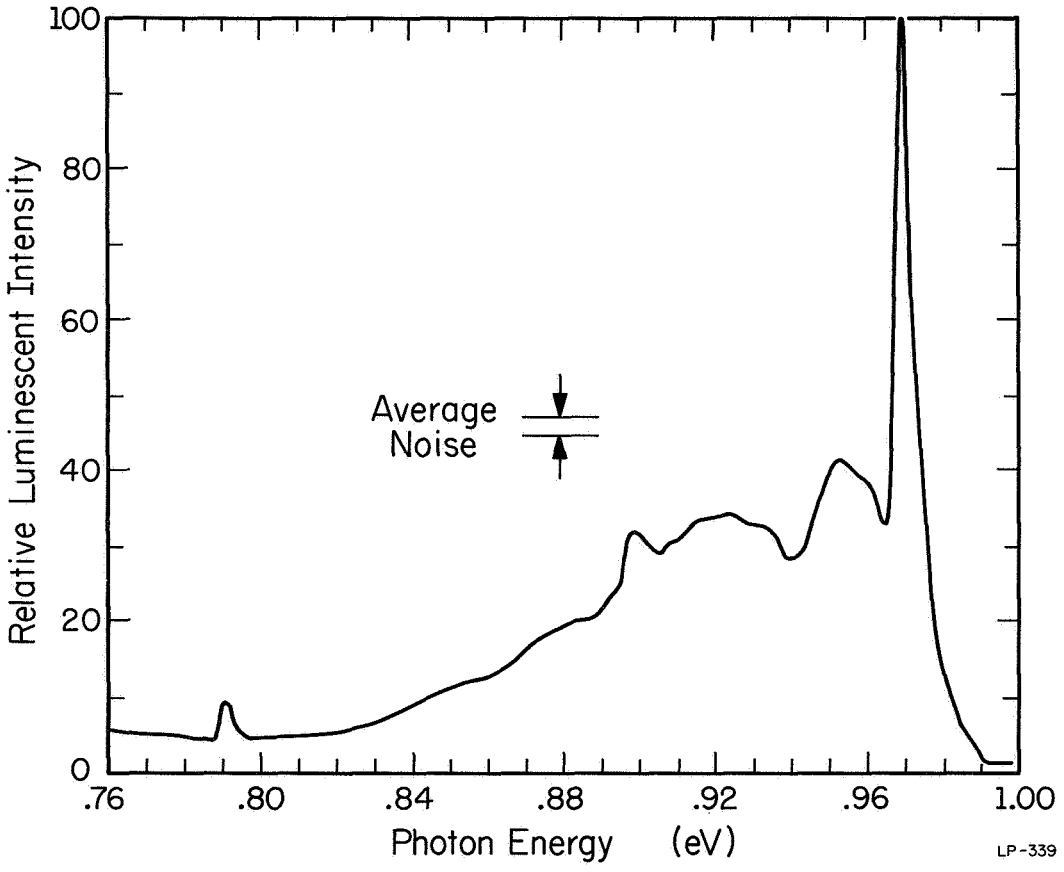
100
80
60
40
20
0
Relative Luminescent Intensity
Average
Noise
.76
.80
.84
.88
.92
.96
1.00
Photon Energy (eV)
LP-339

Figure 7

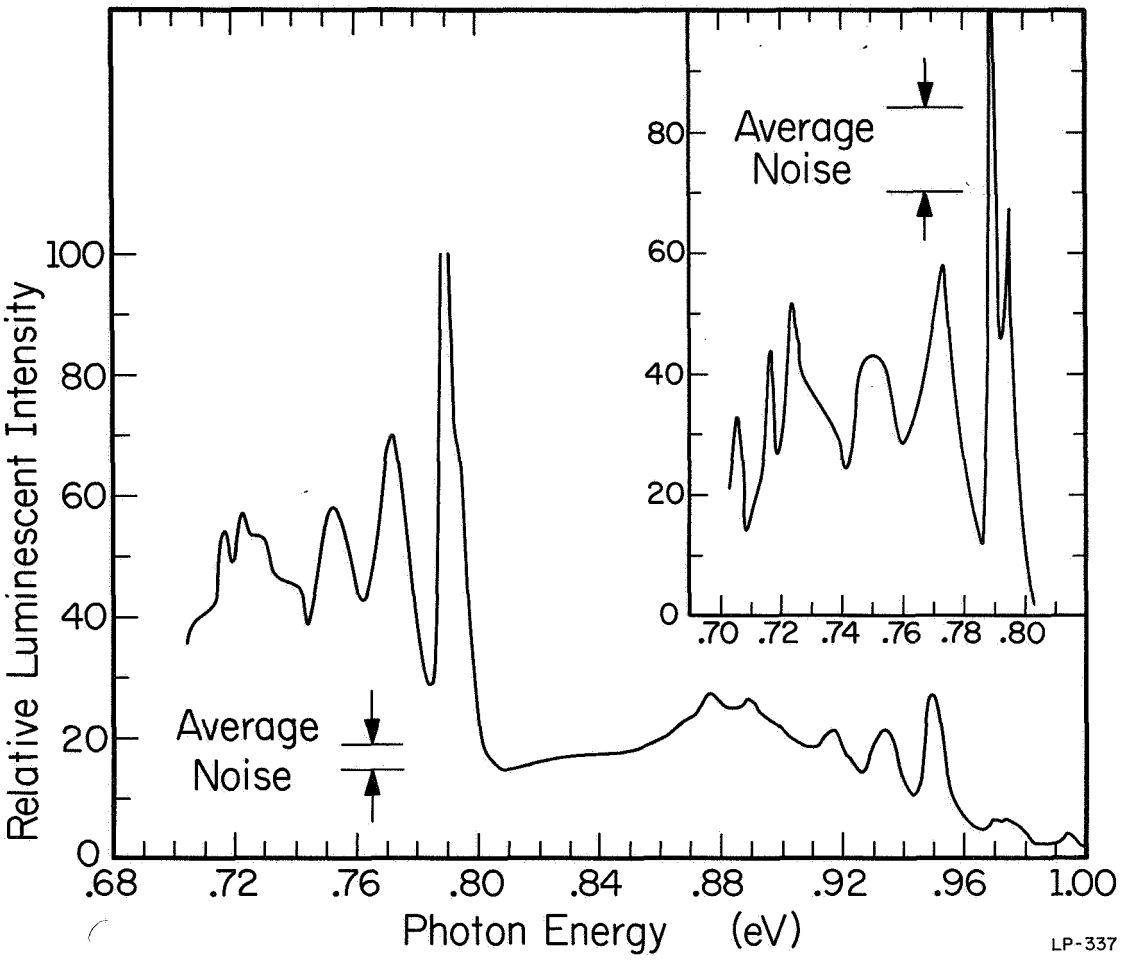
Relative Luminescent Intensity
100
80
60
40
20
0
.68
.72
.76
.80
.84
.88
.92
.96
1.00
Photon Energy (eV)
Average Noise
Average Noise
80
60
40
20
0
.70
.72
.74
.76
.78
.80
LP-337

Figure 8

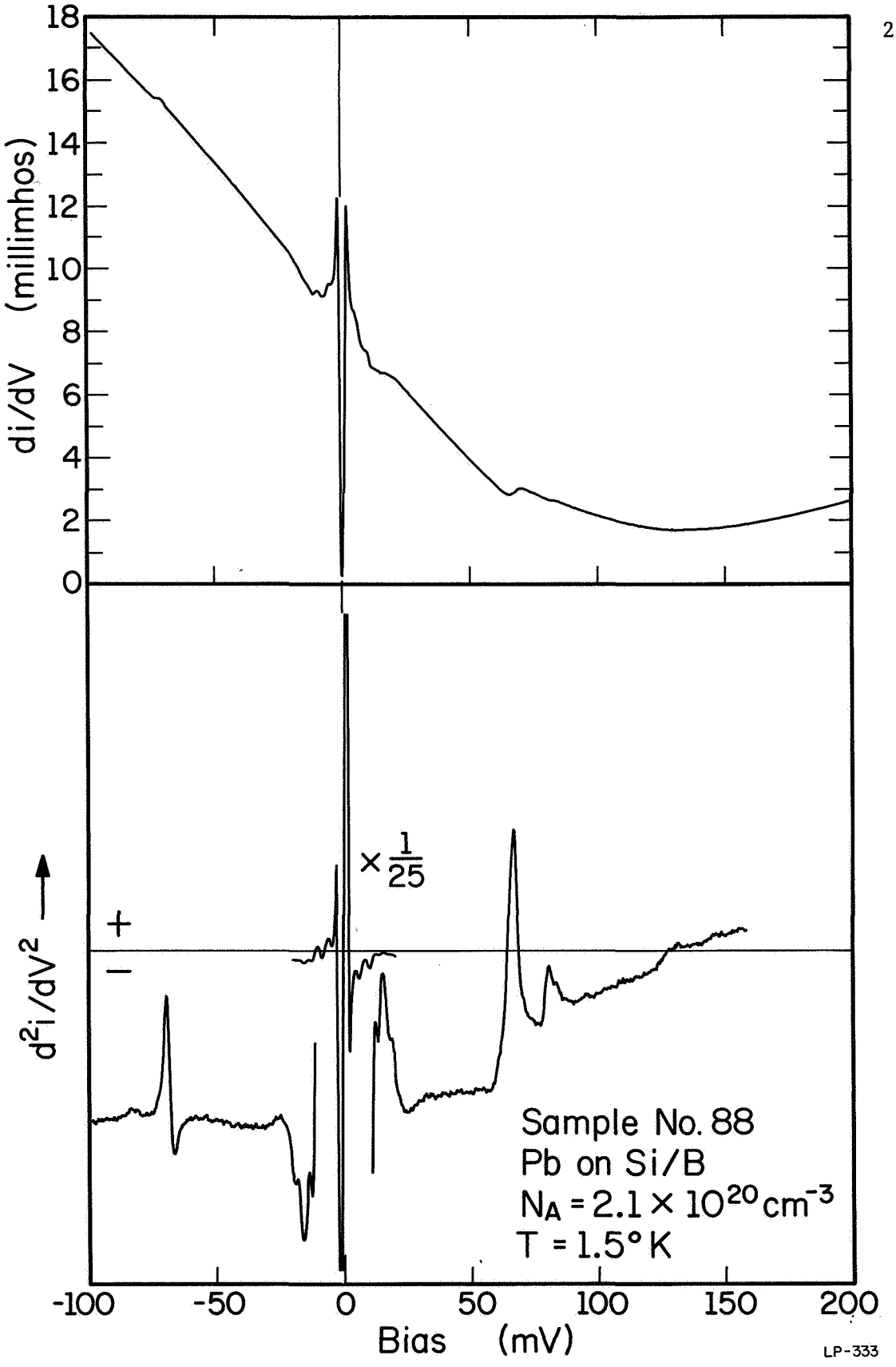
18
16
14
12
10
8
6
4
2
0
di/dV (millimhos)
× 1/25
+
−
d²i/dV² →
Sample No. 88
Pb on Si/B
N_A = 2.1 × 10^20 cm^-3
T = 1.5° K
-100
-50
0
50
100
150
200
Bias (mV)
LP-333

Figure 9

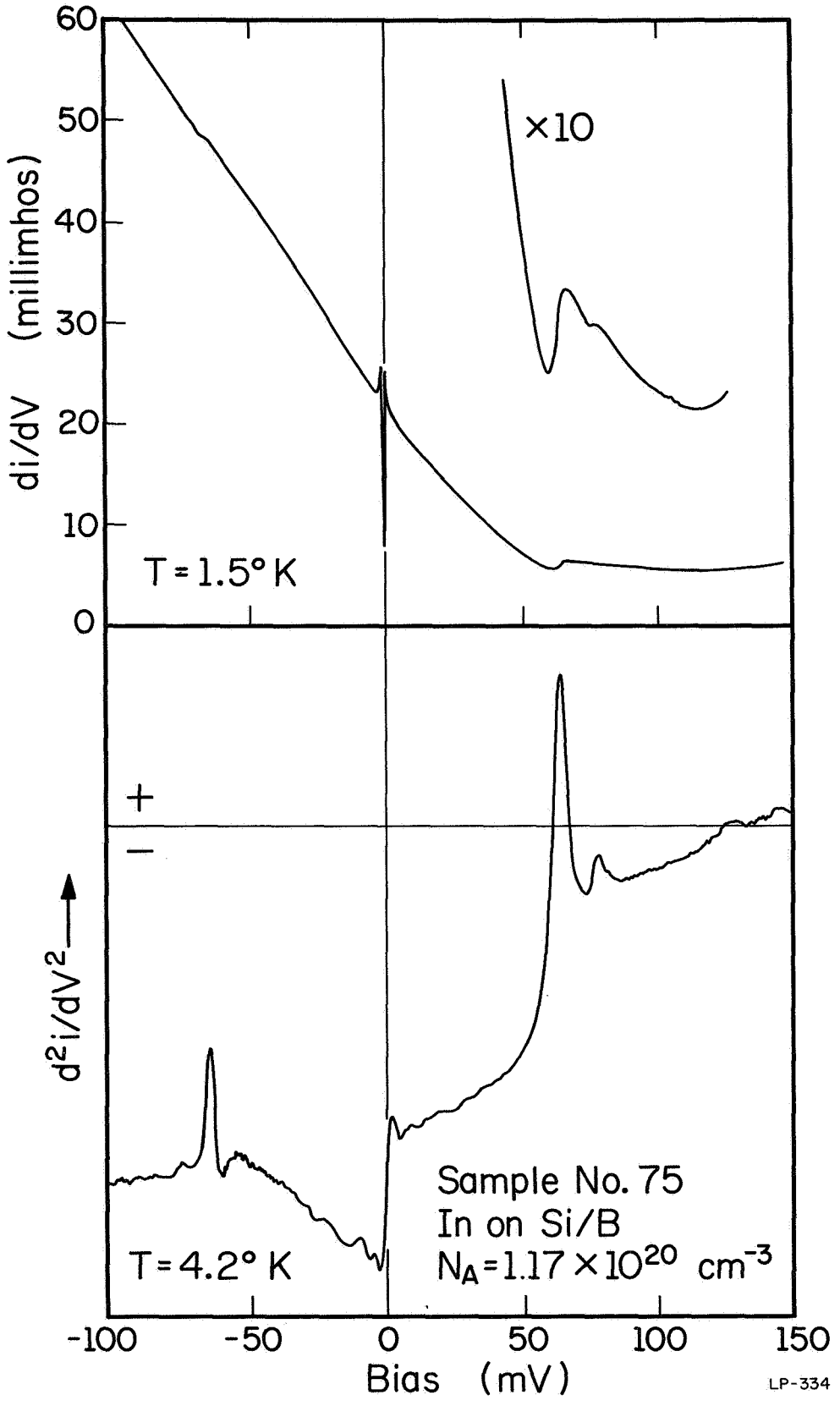
60
50
40
30
20
10
0
di/dV (millimhos)
×10
T = 1.5° K
+
−
d²i/dV²
Sample No. 75
In on Si/B
N_A = 1.17 × 10^20 cm^-3
T = 4.2° K
-100
-50
0
50
100
150
Bias (mV)
LP-334

Figure 10

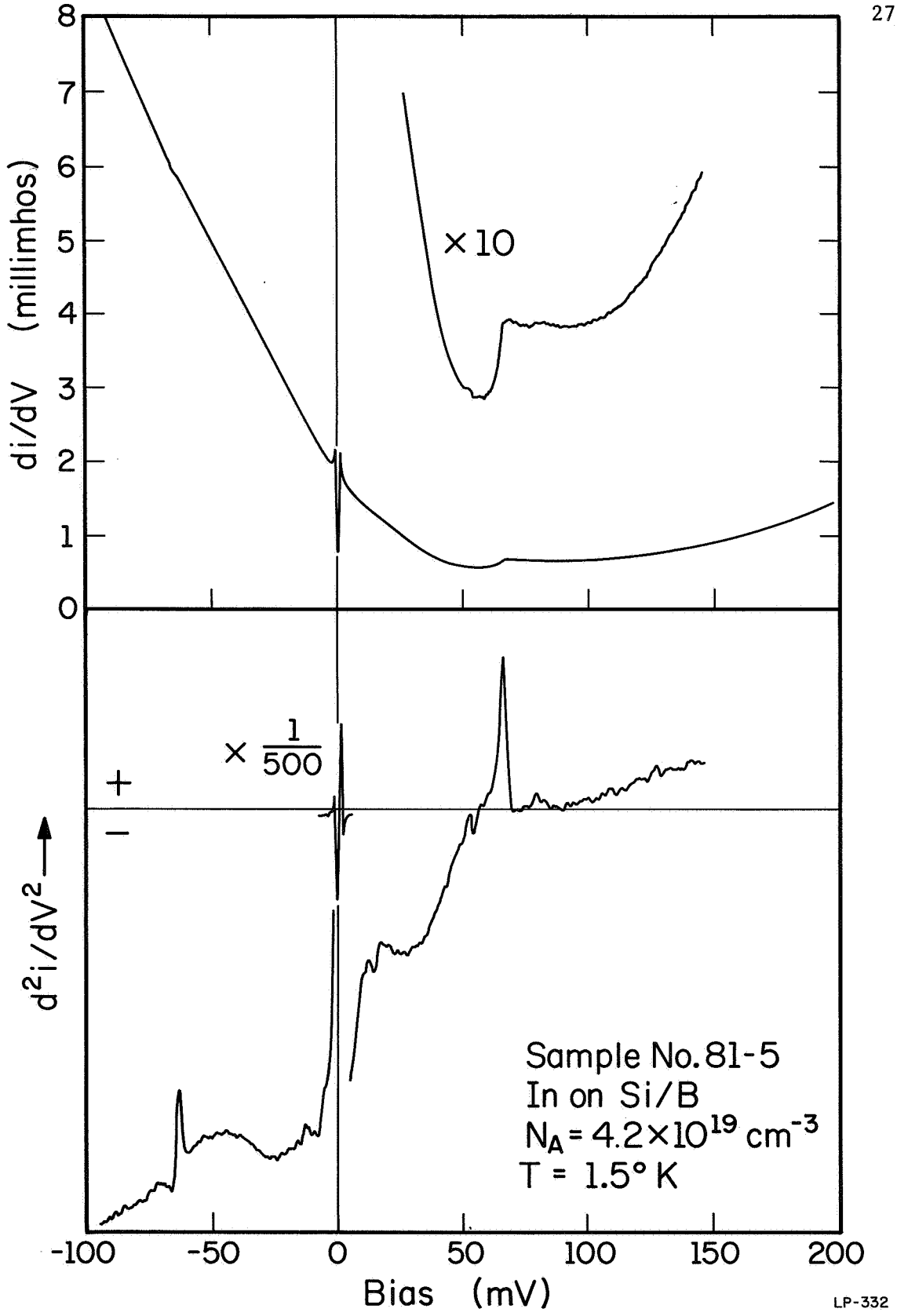
di/dV (millimhos)
8
7
6
5
4
3
2
1
0
×10
× 1/500
+
−
d²i/dV²
Sample No. 81-5
In on Si/B
N_A = 4.2×10^19 cm^-3
T = 1.5° K
-100
-50
0
50
100
150
200
Bias (mV)
LP-332

Figure 11

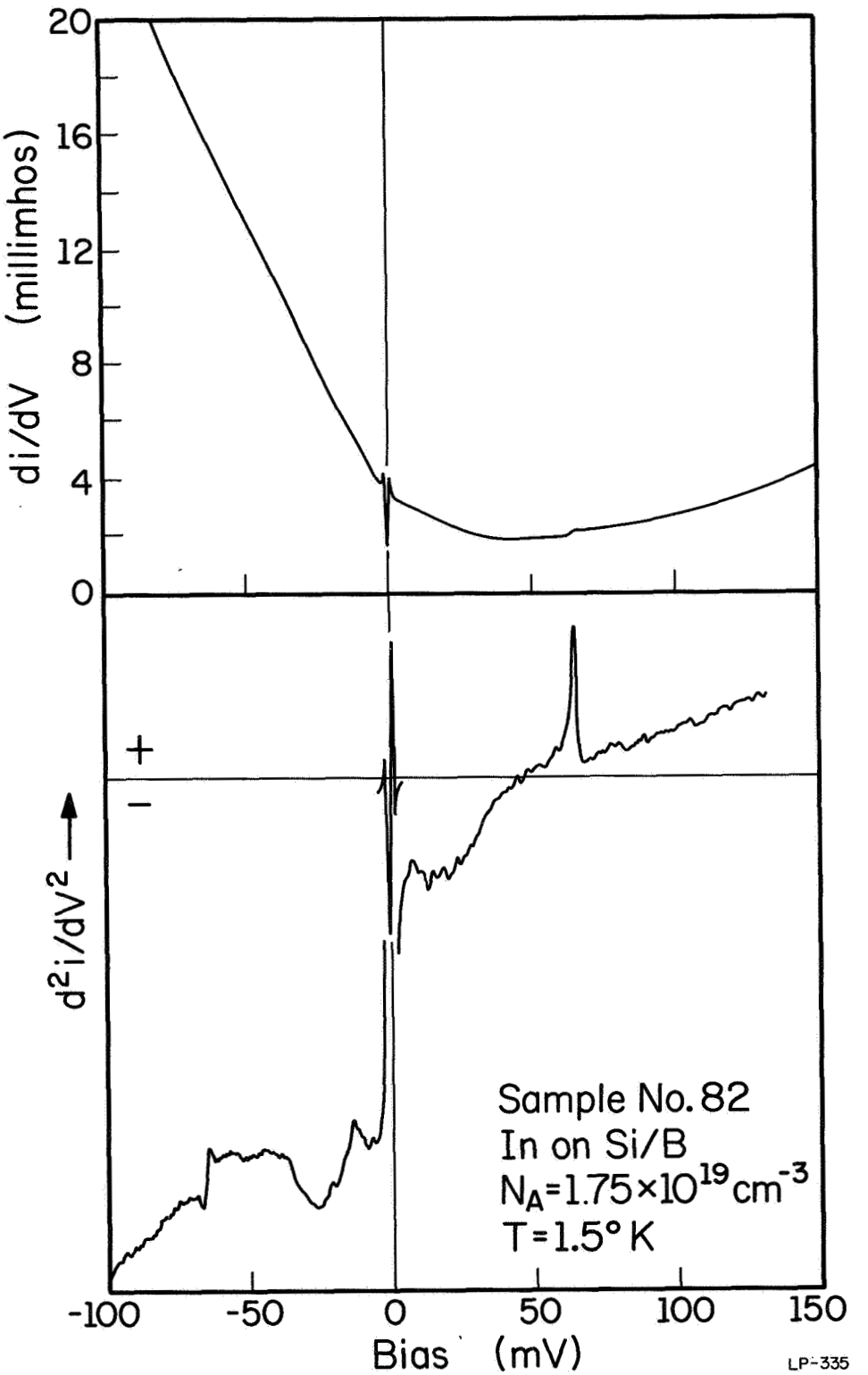
20
16
12
8
4
0
di/dV (millimhos)
+
−
d^2i/dV^2
Sample No. 82
In on Si/B
$N_A=1.75\times10^{19}cm^{-3}$
T=1.5° K
-100
-50
0
50
100
150
Bias (mV)
LP-335

Figure 12

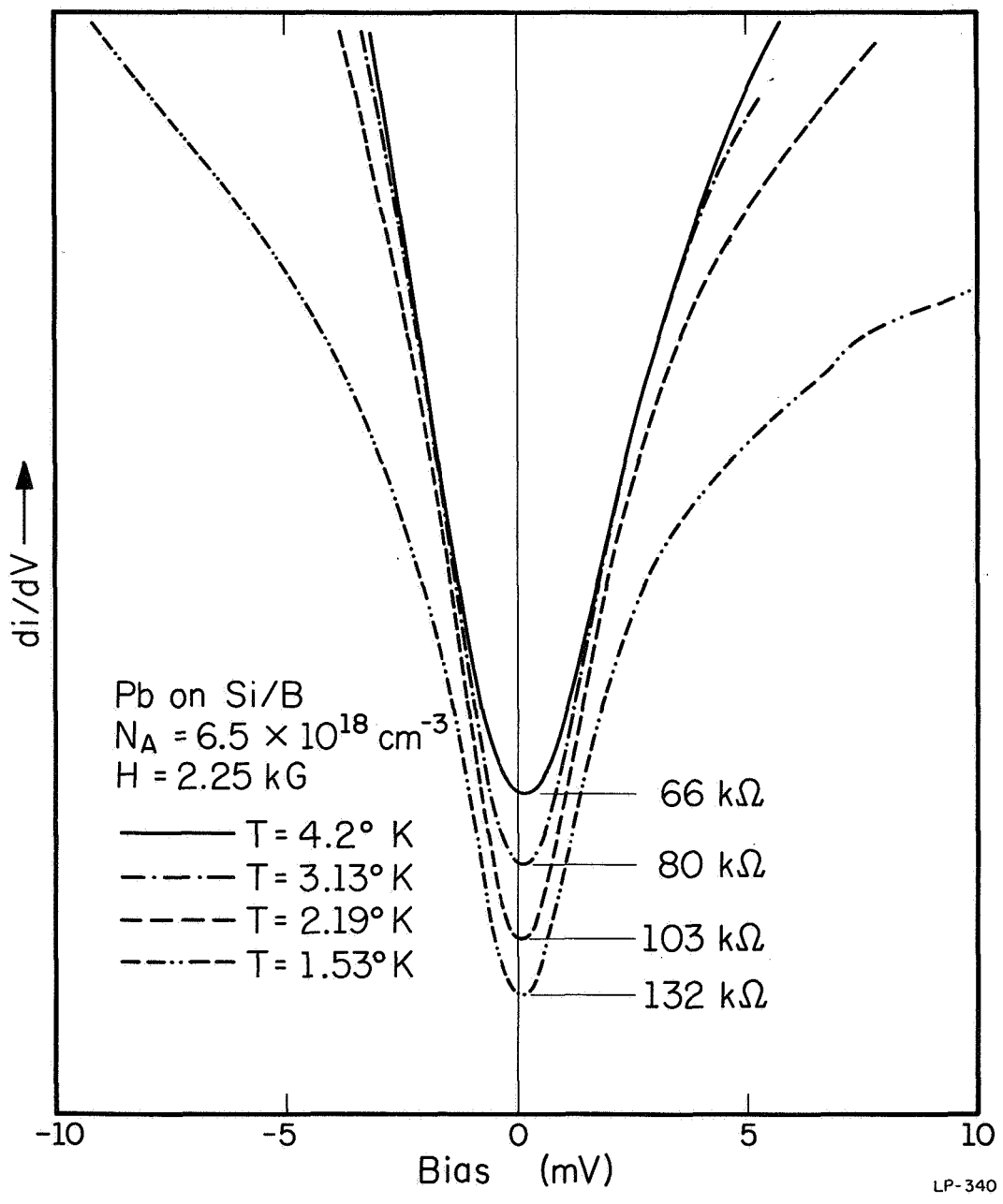
di/dV
Pb on Si/B
$N_A = 6.5 \times 10^{18}$ cm^{-3}
H = 2.25 kG
T = 4.2° K
T = 3.13° K
T = 2.19° K
T = 1.53° K
66 kΩ
80 kΩ
103 kΩ
132 kΩ
-10
-5
0
5
10
Bias (mV)
LP-340

Figure 13

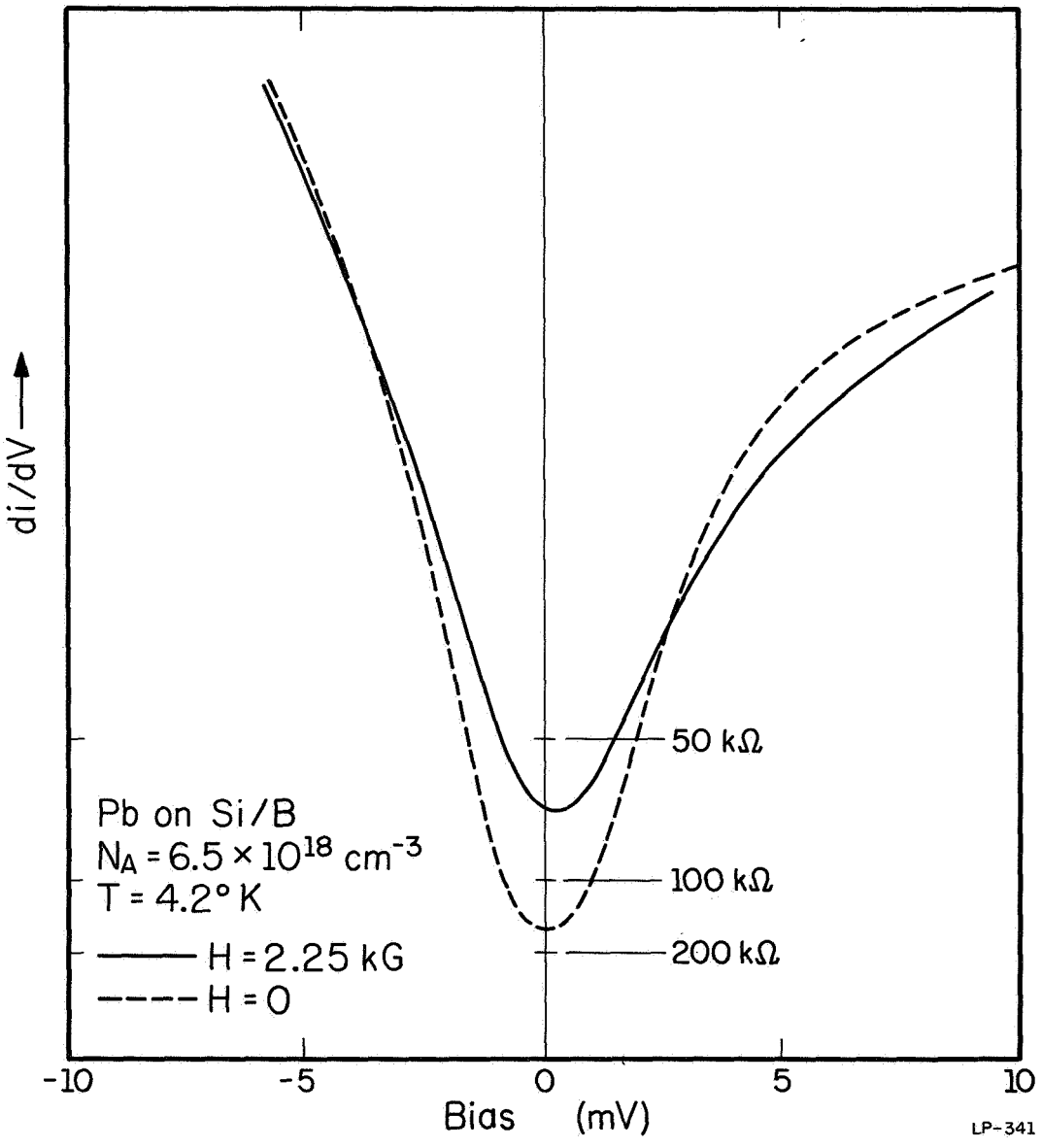
di/dV
Pb on Si/B
$N_A = 6.5 \times 10^{18}$ cm^{-3}
T = 4.2° K
H = 2.25 kG
H = 0
50 kΩ
100 kΩ
200 kΩ
-10
-5
0
5
10
Bias (mV)
LP-341

Figure 14